

AD-A081 462

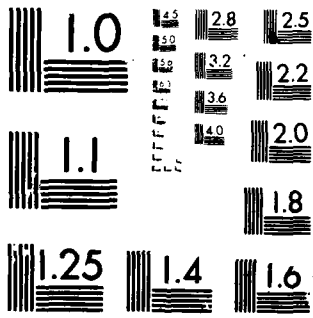
CALIFORNIA UNIV SAN DEIGO LA JOLLA DEPT OF ELECTRICA--ETC F/G 3/2
THE LATITUDINAL STRUCTURE OF SOLAR WIND STREAMS FROM RADIO SCIN--ETC(U)
SEP 79 S ANANTHAKRISHNAN, W A COLES F19628-77-C-0161
SCIENTIFIC-2 AFGL-TR-79-0234 NL

UNCLASSIFIED

[OF]
dt
SUBMIT



										END DATE FILMED 4-80 DTIC		



MICROCOPY RESOLUTION TEST CHART
NATIONAL BUREAU OF STANDARDS-1963-A

AFGL-TR-79-0234

THE LATITUDINAL STRUCTURE OF
SOLAR WIND STREAMS FROM
RADIO SCINTILLATION OBSERVATIONS

S. Ananthakrishnan
W.A. Coles
J.J. Kaufman
B.J. Rickett

Department of Electrical Engineering
and Computer Sciences
University of California, San Diego
La Jolla, California 92093

Scientific Report No. 2

September 1979

Approved for public release; distribution unlimited

AIR FORCE GEOPHYSICS LABORATORY
AIR FORCE SYSTEMS COMMAND
UNITED STATES AIR FORCE
HANSCOM AFB, MASSACHUSETTS 01731

DTIC
ELECTE
MAR 6 1980

411 629

80 3 4 004

AD A081462

DDC FILE COPY

Qualified requestors may obtain additional copies from the Defense Documentation Center. All others should apply to the National Technical Information Service.

Unclassified

SECURITY CLASSIFICATION OF THIS PAGE (When Data Entered)

19 REPORT DOCUMENTATION PAGE		READ INSTRUCTIONS BEFORE COMPLETING FORM	
1. REPORT NUMBER AFGL-TR-79-0234	2. GOVT ACCESSION NO.	3. RECIPIENT'S CATALOG NUMBER	
4. TITLE (and Subtitle) THE LATITUDINAL STRUCTURE OF SOLAR WIND STREAMS FROM RADIO SCINTILLATION OBSERVATIONS		5. TYPE OF REPORT & PERIOD COVERED Scientific Report 21	
7. AUTHOR(s) S./Ananthakrishnan B. J./Rickett W. A./Coles J. J./Kaufman		8. CONTRACT OR GRANT NUMBER(s) F19628-77-C-0161	
9. PERFORMING ORGANIZATION NAME AND ADDRESS Dept of Electrical Engineering and Computer Sciences University of California, San Diego La Jolla, California 92093		10. PROGRAM ELEMENT, PROJECT, TASK AREA & WORK UNIT NUMBERS 61102F 2311G3AD	
11. CONTROLLING OFFICE NAME AND ADDRESS Air Force Geophysics Laboratory Hanscom AFB, Massachusetts 01731 Monitor/Richard C. Altrock/PHS		12. REPORT DATE Sep 1979	
14. MONITORING AGENCY NAME & ADDRESS (if different from Controlling Office) 12 35		13. NUMBER OF PAGES 34	
		15. SECURITY CLASS. (of this report) Unclassified	
		15a. DECLASSIFICATION/DOWNGRADING SCHEDULE	
16. DISTRIBUTION STATEMENT (of this Report) Approved for public release; distribution unlimited			
17. DISTRIBUTION STATEMENT (of the abstract entered in Block 20, if different from Report)			
18. SUPPLEMENTARY NOTES			
19. KEY WORDS (Continue on reverse side if necessary and identify by block number)			
20. ABSTRACT (Continue on reverse side if necessary and identify by block number) We present a comparison of spacecraft and IPS measurements of the solar wind velocity for 1973-75, when the large scale velocity structure was very stable. From this comparison we infer a prototype distribution across a			

DD FORM 1473
1 JAN 73

EDITION OF 1 NOV 65 IS OBSOLETE

Unclassified 411629

SECURITY CLASSIFICATION OF THIS PAGE (When Data Entered)

high speed stream for the electron density fluctuations, Δn_e , in the spatial frequency range $10^{-4} - 10^{-2} \text{ km}^{-1}$. The "microturbulence" is more closely related to the velocity structure in a stream than to the bulk density; enhancements in Δn_e occur wherever high speed wind overtakes low speed wind. The distribution of Δn_e is closely matched by the distribution of magnetic field fluctuations $\sim 10^{-6} \text{ km}^{-1}$.

Unclassified

Preface

Since 1972 the UCSD 74-MHz radio observatory has continuously monitored the solar wind over a wide range in heliographic latitude using the method of interplanetary scintillations (IPS). A primary goal has been to study the connection between high speed streams, which cause geomagnetic disturbances, and the structure of the lower corona. In this report we present in preprint form two papers which examine certain aspects of this investigation. The first, "Microturbulence in Solar Wind Streams", discusses the interpretation of the velocity measured by IPS, which is a path-smoothed version of the point solar wind velocity. This work provides a prototype line-of-sight smoothing function which can be used to infer point velocities from IPS data in regions where spacecraft measurements are not available. The second paper, "Solar Cycle Changes in the High Latitude Solar Wind", reports the discovery of a systematic variation with the sunspot cycle of the average high latitude velocity. This variation is explained by relating it to changes in the gross magnetic field structure in the lower corona.

Contents

	Page
Microturbulence in Solar Wind Streams S. Ananthakrishnan, W.A. Coles, J.J. Kaufman, and B.J. Rickett	1
Solar Cycle Changes in the High Latitude Solar Wind S. Ananthakrishnan, W.A. Coles, J.J. Kaufman, and B.J. Rickett	19

"Microturbulence in Solar Wind Streams"

S. Ananthakrishnan, W.A. Coles and J.J. Kaufman

Abstract

(Interplanetary scintillations)

~~We present~~ ^{are presented} a comparison of spacecraft and IPS measurements of the solar wind velocity for 1973-75_A when the large scale velocity structure was very stable. From this comparison we infer a prototype distribution across a ^{delta n sub e} high speed stream for the electron density fluctuations, Δn_e , in the spatial frequency range $10^{-4} - 10^{-2} \text{ km}^{-1}$. The "microturbulence" ^{$1/10,000 - 1/100 \text{ /km}$} is more closely related to the velocity structure in a stream than to the bulk density; enhancements in Δn_e occur wherever high speed wind overtakes low speed wind. The distribution of Δn_e is closely matched by the distribution of magnetic field fluctuations $\sim 10^{-6} \text{ km}^{-1}$. ^{delta n sub e}
 _{approx. $1/1,000,000 \text{ /km}$}

The solar wind velocity estimated from observations of interplanetary scintillations (IPS) can be compared with spacecraft measurements during 1973-75 when the large scale structure was very stable. Coles, Harmon, Lazarus, and Sullivan (1978) made such a comparison using 74 MHz data from the ecliptic source 3C144 both to "calibrate" the IPS data of 1973 and to infer the distribution of the electron density fluctuations which cause IPS. In this paper we have estimated the distribution of this "microturbulence" more precisely using a refined technique, and we have extended the comparison through 1975.

The IPS observed by the UCSD 74 MHz observatory is caused by micro-turbulence of spatial frequency 10^{-4} to 10^{-2} km^{-1} . The level of the fluctuation spectrum in this range, $(\Delta n_e)^2$, appears as a weighting function in the path integral for an IPS observation. Thus to "invert" this integral - that is, to recover the point measurement - one must have accurate knowledge of the distribution of $(\Delta n_e)^2$. Unfortunately Δn_e is not regularly observed by spacecraft because the frequency range is too high, so we must use model-fitting techniques. The IPS observations are reduced to three parameters: the scintillation index, peak velocity, and midpoint velocity. The index is the normalized rms intensity variation. It is proportional to Δn_e in weak scattering, but inversely related to Δn_e in strong scattering. The midpoint velocity gives a weighted mean of the velocity component transverse to the line of sight, whereas the peak velocity selects the higher velocities along this path. These parameters can be calculated in weak scattering (for elongations greater than 40° at 74 MHz) if the velocity and Δn_e are known. The details of this calculation are given by Coles, Harmon, Lazarus, and Sullivan (1978). In strong scattering the velocities calculated are no longer exact (although they are still useful), but the index must be discarded.

In the earlier work, the spacecraft velocities and a model distribution of Δn_e were used to predict the IPS parameters. The predictions were compared with the observations and inferences about the model Δn_e were drawn. A model for which $\Delta n_e \propto n_p$ (the bulk proton density) was tested. This correctly predicted the increases of index which are observed before high speed streams (Houminer and Hewish, 1974), but the velocity agreement was poor. Coles, Harmon, Lazarus, and Sullivan (1978) found that this model overestimated Δn_e in the compression region and underestimated Δn_e in the interior of a stream. Other simple models were tried, but none gave a uniformly good match. We have confirmed these conclusions by extending the earlier analysis through 1975 (see also Harmon, 1975).

Methods

The distribution of microturbulence can be estimated using an iterative process provided, of course, that it converges to a unique solution. Here the IPS parameters are predicted, as before, and the model Δn_e is perturbed until a "best fit" to the observed parameters is obtained. We have used an interactive program in which an operator judges the goodness-of-fit from a graphics display and specifies the next perturbation on this display. This was necessary to speed convergence and to permit certain features of the data, such as the rising edge of a high speed stream, to be emphasized. It also permits us to ignore doubtful data points, but makes the process somewhat subjective. We applied this process to data of 1973-75 using two fitting criteria. First we matched only the peak and midpoint velocities, ignoring the indices. This process converged, but occasionally two quite different solutions were possible. We then matched all three parameters simultaneously. This additional constraint eliminated the ambiguities and improved the convergence. It was found that

introducing the index did not degrade the agreement between predicted and observed velocities. Thus the index is indeed acting as a constraint, and it is consistent with the velocity data. We used the index as secondary data because its sensitivity to interference is greater and it cannot be used in strong scattering.

The prediction calculation is done exactly as described by Coles, Harmon, Lazarus, and Sullivan (1978). It includes a power-law density spectrum with an exponent of -2.7 as described by Coles and Harmon (1978); it includes the radio source structure; it uses a solar distance dependence $\Delta n_e \propto r^{-2}$ (Armstrong and Coles, 1978); and it uses a simple spiral model to map spacecraft data to the line of sight. As before, no allowance is made for stream evolution (with distance or time), and heliographic latitude differences of up to 7° are ignored. The spacecraft data used in the calculations has 6-hour resolution, and the iterative process is applied to overlapping 30-day blocks of data. The initial guess of $\Delta n_e \propto n_p$ is perturbed first to match the velocity, then to match the index without degrading the velocity match. The final result is an estimate of the microturbulence, Δn_e , for 1973-75, which can be compared directly with spacecraft plasma and magnetic field data.

Results

The spacecraft velocity and density; the IPS parameters; and the Δn_e estimates for 1973-75 are shown in Figures 1-3. Only the midpoint velocity is shown, as it is representative of the velocity match and is more sensitive to Δn_e than is the peak velocity. Spacecraft (IMP 6, 7 and 8) data gaps, indicated by x's, were filled by linear interpolation. The measured IPS data, indicated by x's, are overplotted on the model calculation,

and generally good agreement can be seen. For comparison, results for the "initial guess" model, $\Delta n_e \propto n_p$, are also shown. During this entire period the persistence of the overall velocity structure is strong, especially during 1974 when two streams remain stable for at least 7 rotations. However, there are significant changes in the streams, particularly in n_p and Δn_e at their leading edges, even when the velocity structure repeats well.

A major cause of error is the "noise" on the IPS observation. There is a random component simply due to receiver noise and systematic component caused by interference. These are most important when the scintillations are weak - that is, when the solar elongation is large (greater than 120°) or small (less than 20°). Interference always increases the apparent scintillation index but will only affect the velocities if it is correlated over the 100 km spacing between antennas. Solar radio bursts cause correlated interference with zero time lag, and thus the velocity tends to be overestimated; otherwise there is no significant bias to the velocity, although the errors do increase as the scintillation decreases. Typical estimation errors are 10% for the velocity and 30% for the index.

There are periods in Figures 1-3 where a satisfactory match could not be obtained for an Δn_e model. For example, near days 210 and 235 of 1974 the velocity and index could be matched separately but not simultaneously. Here a compromise is shown, but it is clear that one of our assumptions has broken down. Occasionally the velocity cannot be matched by any model. For example near day 80 of 1974 the IPS velocities are lower than any calculation, whereas near day 220 of 1974 the reverse is true. There are several cases, such as days 113 and 238 of 1973, where rapid changes occur in both the spacecraft and IPS velocities but do not appear in the predictions (which have a

smoothing effect). These discrepancies can be caused by temporal variations, stream evolution, or latitude differences, but they do not affect a significant fraction of the data.

The "best fit" model for Δn_e shown in Figures 1-3 has an amplitude error comparable with that of the index, about 30%. However the leading edges of the enhancements are located quite accurately; the error is about 6 hrs. Details of the model in the falling portion of a stream are less reliable. Here the velocity is changing slowly, so a change in the distribution of Δn_e has little effect.

The comparisons of Figures 1-3 are summarized in Table 1. Results for both the midpoint ("mid") and peak ("pk") velocities are shown. Table 1 gives the average velocity \bar{v} , the standard deviation σ_v , the correlation coefficient ρ_v between the observed and model velocities, and the rms difference ϵ_v between these velocities. The IPS standard deviations and the ρ 's and ϵ 's are all corrected for estimation error in the data. For comparison, the average spacecraft velocity was 499 km s^{-1} and its standard deviation 128 km s^{-1} . The correlation coefficient ρ_m between the observed and model scintillation indices is also shown. It was calculated after removing a low frequency trend from both the data and the model indices.

Discussion

Differences of detail from stream to stream are less important than the general character of the Δn_e distribution. This is shown in Figure 4, which gives a superposed epoch average of 23 streams aligned by the density maximum at the leading edge. The Δn_e profile can be compared with epoch averages of other plasma parameters or used as a prototype weighting function when interpreting IPS data.

In Figure 4 the Δn_e model attains a maximum twice its average value 12 hours behind the density peak. It decays slowly inside the stream, falling below its average value after four days. In contrast, the proton density fluctuations, σ_{n_p} , follow the bulk density. σ_{n_p} is dominated by spatial frequencies $\sim 10^{-6} \text{ km}^{-1}$. Thus the difference between σ_{n_p} and Δn_e indicates that the shape of the fluctuation spectrum changes systematically as a stream passes. At the density maximum, the spectrum steepens relative to its pre-stream configuration; then it flattens inside the stream before relaxing back to its original shape.

In Figure 5 we divide the streams into two groups according to width. The broad streams have the broader Δn_e enhancement, as though high speed wind were intrinsically more turbulent than low speed wind. However, our data from high latitude sources do not support this interpretation. These sources, which are observed through faster wind than in the ecliptic (Coles and Rickett, 1976), show scintillation index variations with elongation that are indistinguishable from those of ecliptic sources. Furthermore, there is no apparent difference between index data of 1972 and 1974, although the average ecliptic velocity differed by $\sim 100 \text{ km s}^{-1}$ (Feldman, Asbridge, Bame, and Gosling, 1978).

The extended Δn_e enhancement in the broad streams appears to be related to the internal velocity structure, which was more complex than in narrow streams. To illustrate, we have calculated an epoch average of the positive velocity gradient, ∇V^+ , which is defined to be zero if the velocity is decreasing. If a constant is added to ∇V^+ , as in Figure 5, a good match to Δn_e is obtained. Apparently, then, Δn_e is enhanced in regions where high speed wind is overtaking low speed wind. The enhancements contribute about 40% of the total micro-turbulence. They may be caused by a process unique to regions of increasing velocity, or they may simply reflect the local amplification of processes

occurring everywhere. If indeed the strength of the enhancements is determined by the velocity gradient, their variation with solar distance may be slower than r^{-2} , since a stream's velocity profile steepens with increasing r . Furthermore, the enhancements will likely be less pronounced out of the ecliptic, where stream-stream interactions are weaker.

Figure 5 also shows the proton temperature, T_p , and the magnetic field fluctuations, σ_B^+ . Both T_p and Δn_e are enhanced inside the stream, but their rising and falling edges do not coincide. σ_B^+ and Δn_e , however, appear to be closely connected. σ_B^+ is measured at frequencies $\sim 10^{-6} \text{ km}^{-1}$, but the distribution of field fluctuations at higher frequencies is probably similar (Behannon, 1976). If so, it is possible that Δn_e is physically connected to a particular type of field activity, for example fluctuations due to hydromagnetic waves. The low frequency field fluctuations have a large Alfvénic component that is especially pure in high speed wind (Belcher and Davis, 1972). However, Alfvén waves cause only weak density fluctuations and thus are unlikely to produce appreciable turbulence directly (Wu and Huba, 1975). On the other hand, they could provide a driving mechanism for the production of high frequency, turbulence-producing waves in regions of overtaking wind.

Attempts to identify such high frequency waves indicate that the situation is complex. Unti and Russell (1976), for example, find little coherence between high frequency plasma flux and field data, indicating that relatively pure waveforms may be rare. However, Behannon (1976) tentatively identifies specific examples of ion cyclotron waves, and Neugebauer, Wu, and Huba (1978) show from statistical arguments that the levels of the flux and field spectra of Unti and Russell (1976) are sometimes consistent with the predictions for magnetosonic waves. But the latter also find evidence for non-wave field and

density irregularities which are maintained by internal pressure balance and convected rigidly at the bulk speed. None of these investigators discusses regions of increasing velocity separately, so there is no information as to the characteristics of the field fluctuations associated with the Δn_e enhancements.

We plan to use the Δn_e profile of Figure 4 as a known weighting factor in an attempt to determine point solar wind velocities from the observed sequence of IPS velocities when spacecraft data is not available. We will concentrate on non-ecliptic regions using 1973-75 data from high latitude sources. This investigation should also reveal the extent to which the prototype ecliptic Δn_e profile is appropriate for high latitudes.

TABLE 1. Comparison of Δn_e model predictions with IPS data

	\bar{V}_{mid} $km\ s^{-1}$	$\sigma_{V_{mid}}$ $km\ s^{-1}$	$\rho_{V_{mid}}$	$\epsilon_{V_{mid}}$ $km\ s^{-1}$	\bar{V}_{pk} $km\ s^{-1}$	$\sigma_{V_{pk}}$ $km\ s^{-1}$	$\rho_{V_{pk}}$	$\epsilon_{V_{pk}}$ $km\ s^{-1}$	ρ_m
IPS DATA	439	108	----	----	470	109	----	----	----
Final Δn_e Model	445	102	0.72	78	488	107	0.73	81	0.68
$\Delta n_e \propto n_p$	397	92	0.47	112	454	104	0.60	96	0.40

Figure Captions

Figure 1: Comparison of 1973 IPS midpoint velocity and scintillation index data (the connected X's) with predictions (the solid lines) for $\Delta n_e \propto n_p$ and the final Δn_e model. Linear interpolation in the IMP spacecraft data is denoted by X's. Units for velocity are km s^{-1} ; for proton number density, cm^{-3} ; for Δn_e and scintillation index, arbitrary. Vertical lines denote Carrington rotations.

Figure 2: Same as Figure 1, but for 1974.

Figure 3: Same as Figure 1, but for 1975.

Figure 4: Epoch average profiles for the proton velocity, V ; the proton density, n_p ; the microturbulence model, Δn_e ; and the low frequency proton density fluctuations, σ_{n_p} . σ_{n_p} is an average of 8 streams; the others are averages of 23 streams. Each parameter (except v) is normalized so that one division is equal to the parameter's mean value, which is denoted by a bar. Scales have offset zeroes and alternate from side to side.

Figure 5: Epoch average profiles for narrow and broad streams, showing the proton velocity, v ; the proton density, n_p ; the microturbulence model, Δn_e ; the proton temperature, T_p ; the low frequency magnetic field fluctuations, σ_B^+ ; and the positive velocity gradient, ∇V^+ , to which a constant, c , has been added. The last three are over-plotted with Δn_e (the dashed lines). Each parameter is normalized so that one division is equal to the parameter's mean value

(including both sets of streams), which is indicated by a bar.

Scales have offset zeroes and alternate from side to side.

References

- Armstrong, J.W., and W.A. Coles, Interplanetary scintillation of PSR 0531+21 at 74 MHz, Astrophys. J., 220, 346, 1978.
- Behannon, K., Observations of the interplanetary magnetic field between 0.46 and 1 A.U. by Mariner 10 spacecraft, GSFC X Doc., 692-76-2, Goddard Space Flight Center, Greenbelt, Md., 1976.
- Belcher, J.W., and L. Davis, Jr., Large amplitude Alfvén waves in the interplanetary medium, 2, J. Geophys. Res., 76, 3534, 1972.
- Coles, W.A., and J.K. Harmon, Interplanetary scintillation measurements of the electron density power spectrum in the solar wind, J. Geophys. Res., 83, 1413, 1978.
- Coles, W.A., J.K. Harmon, A.J. Lazarus, and J.D. Sullivan, Comparison of 74-MHz interplanetary scintillation and IMP 7 observations of the solar wind during 1973, J. Geophys. Res., 83, 3337, 1978.
- Coles, W.A., and B.J. Rickett, IPS observations of the solar wind speed out of the ecliptic, J. Geophys. Res., 81, 4797, 1976.
- Feldman, W.C., J.R. Asbridge, S.J. Bame, and J.T. Gosling, Long-term variations of selected solar wind properties: IMP 6, 7, and 8 results, J. Geophys. Res., 83, 2177, 1978.
- Harmon, J.K., Scintillation studies of density microstructure in the solar wind plasma, Ph.D. thesis, University of California, San Diego, La Jolla, 1975.
- Houminer, Z., and A. Hewish, Long-lived sectors of enhanced density irregularities in the solar wind, Planet. Space Sci., 20, 1703, 1972.
- Neugebauer, M., C.S. Wu, and J.D. Huba, Plasma fluctuations in the solar wind, J. Geophys. Res., 83, 1027, 1978.
- Unti, T., and C.T. Russell, On the causes of spectral enhancements in solar wind power spectra, J. Geophys. Res., 81, 469, 1976.
- Wu, C.S., and J.D. Huba, Low frequency fluctuations in the solar wind, I. Theory, Astrophys. J., 196, 849, 1975.

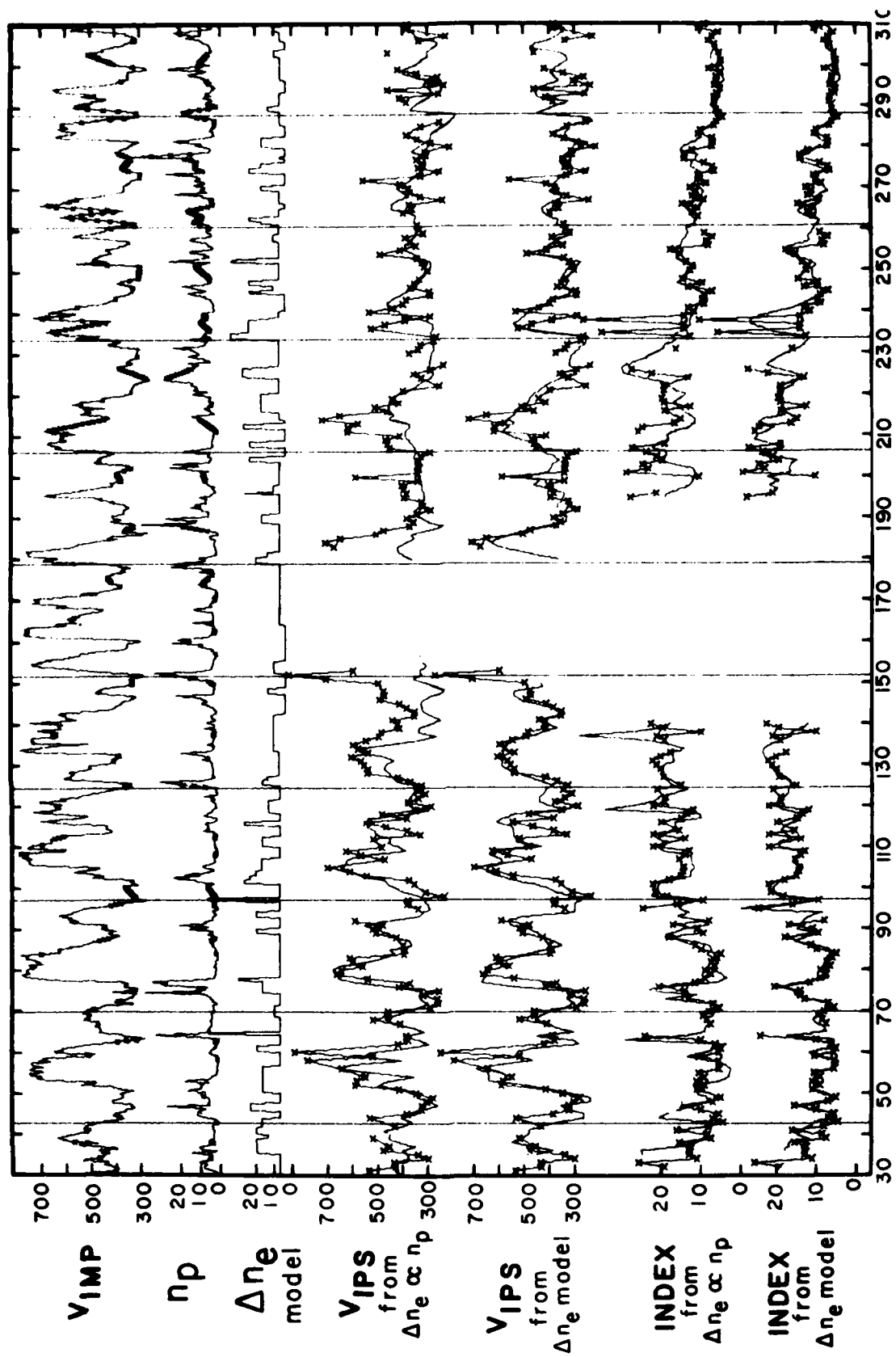


Figure 1.

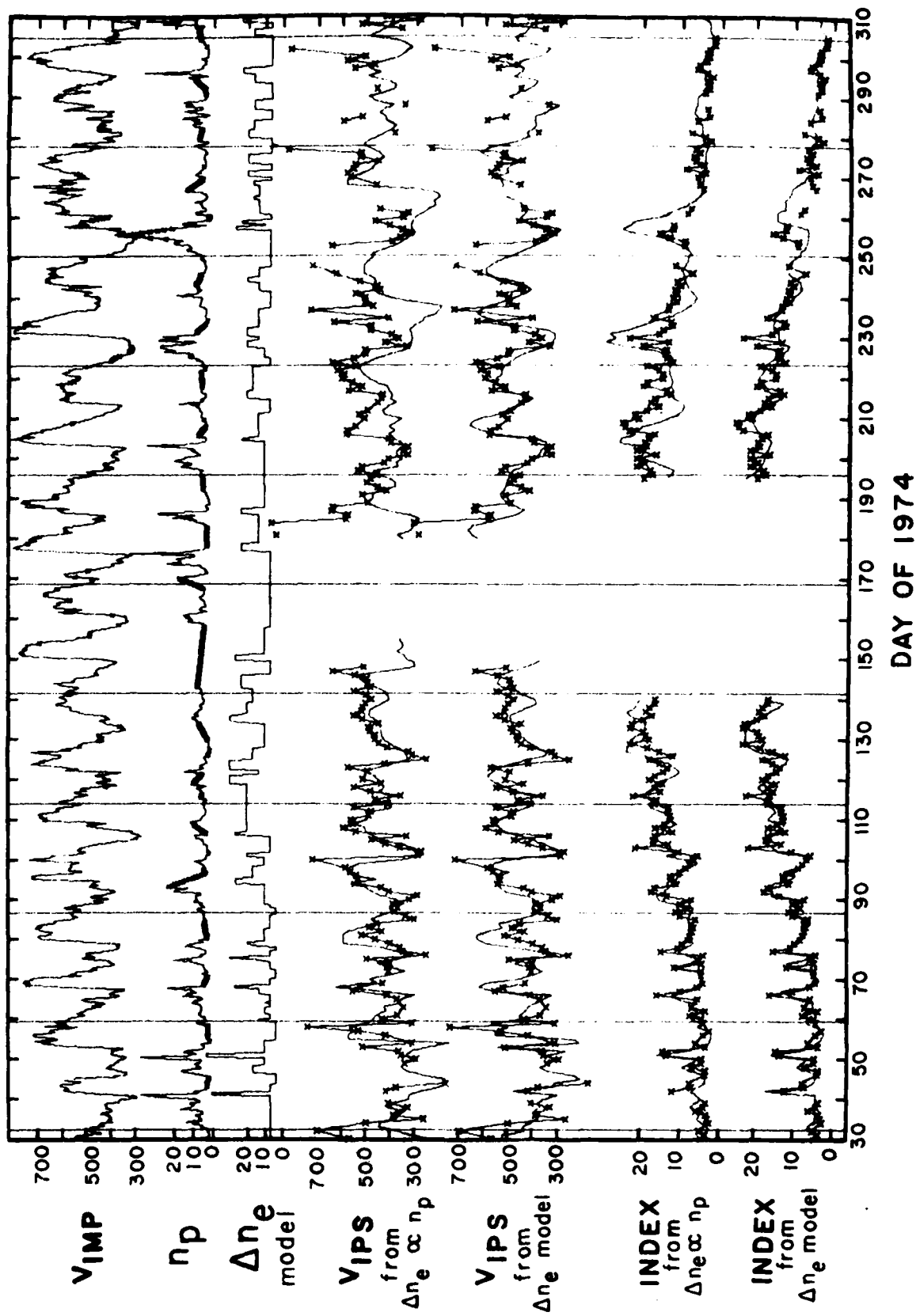


Figure 2.

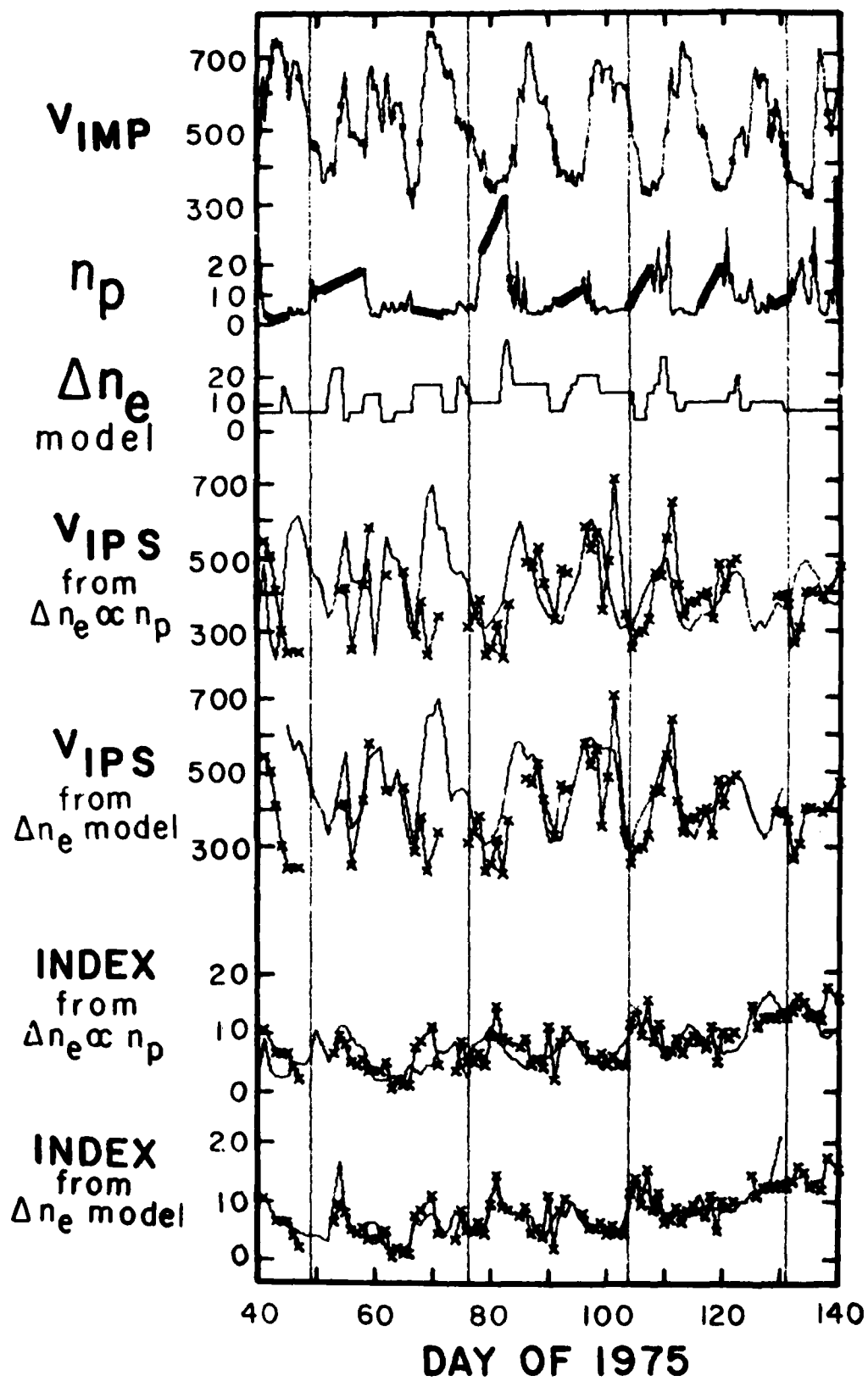


Figure 3.

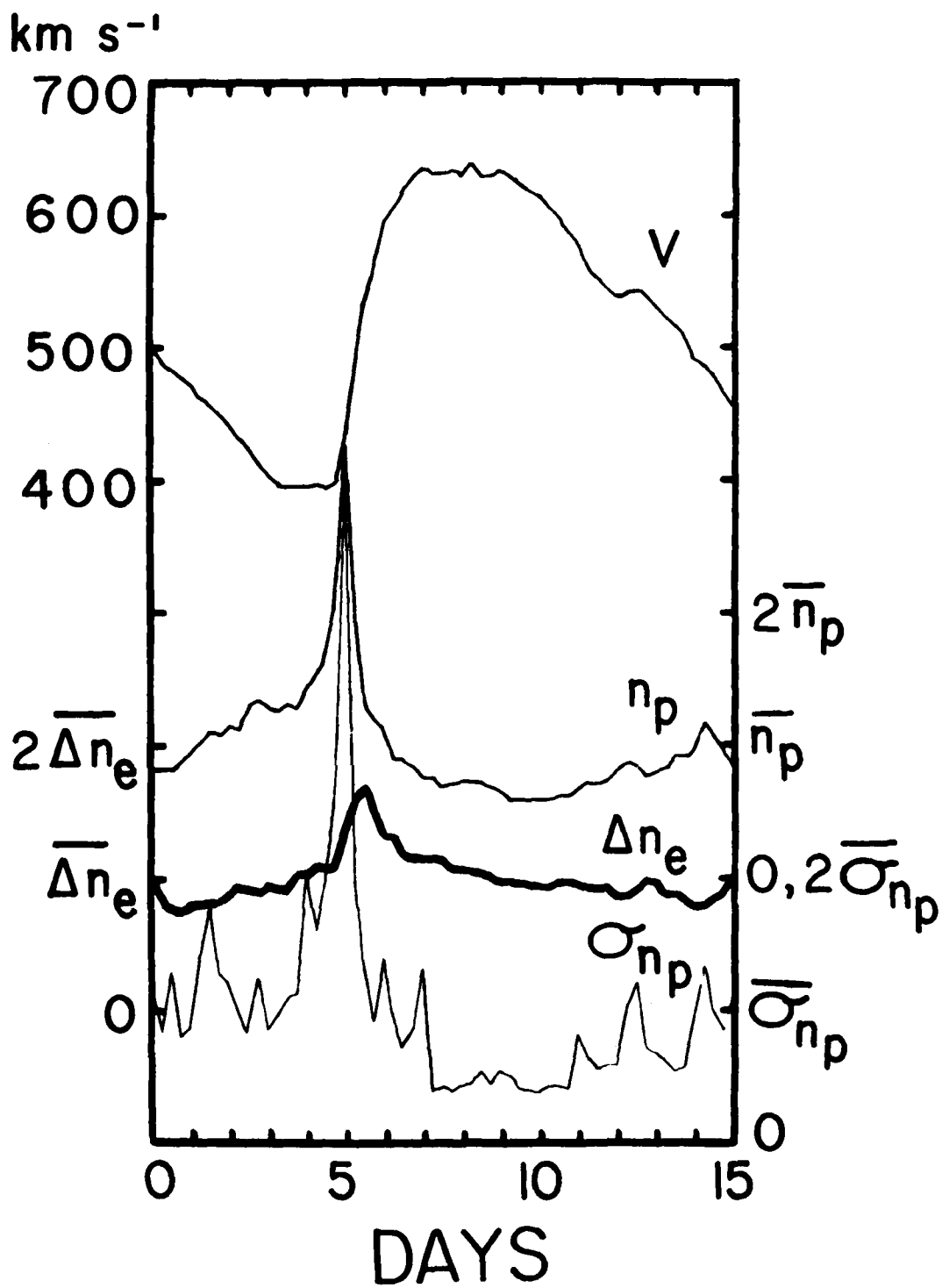


Figure 4.

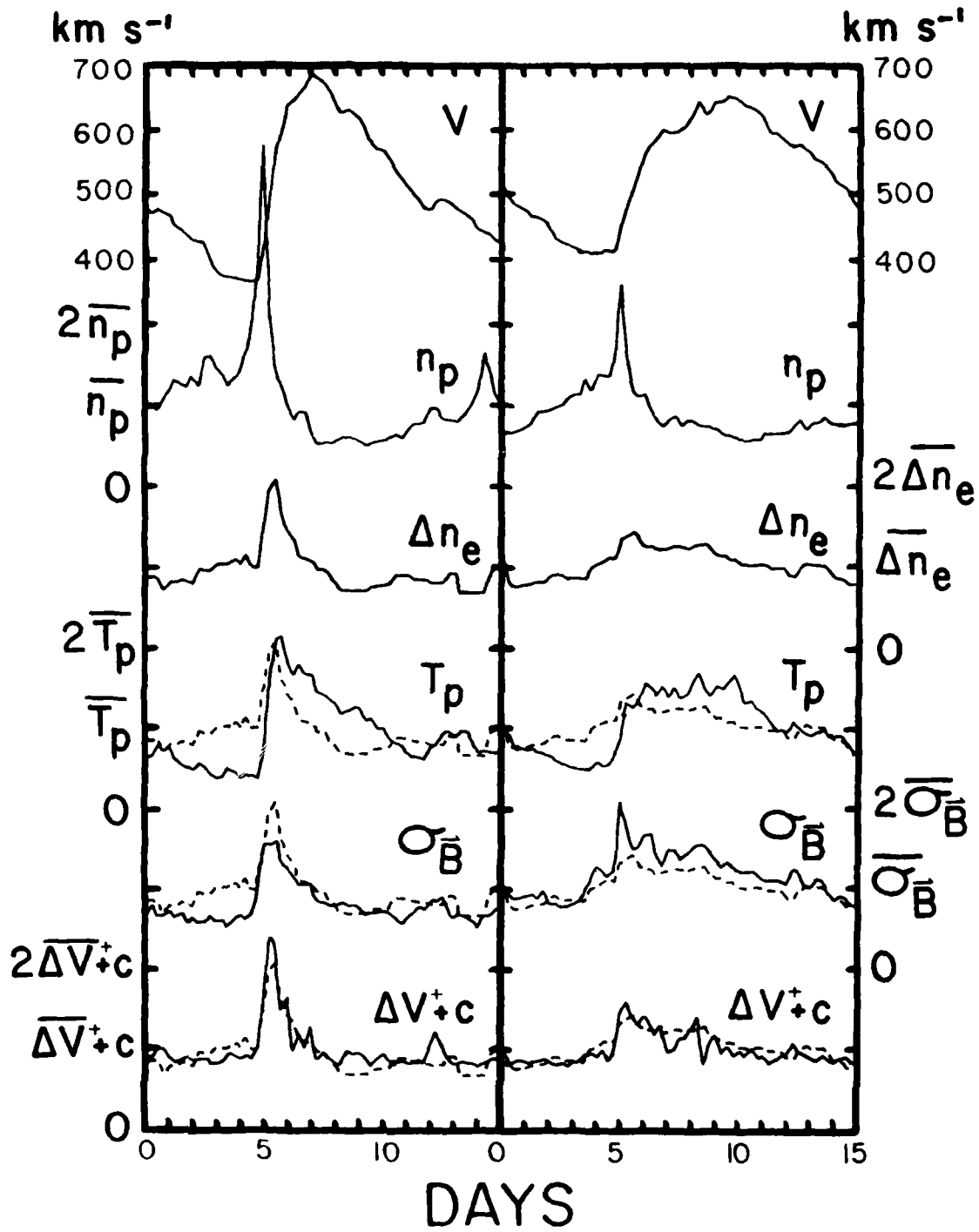


Figure 5.

"Solar Cycle Changes in the
High Latitude Solar Wind"

S. Ananthakrishnan, W.A. Coles, J.J. Kaufman, and B.J. Rickett

Abstract

Measurements of the solar wind speed by the technique of interplanetary scintillation are presented for 1971-79. The average wind speed was faster than 500 km/s at latitudes above $\pm 30^\circ$ for most of 1973-77. This fast polar stream, however, was observed to become much narrower in 1978-79. The narrowing of the polar streams coincided with the emergence of sunspots at mid-latitudes, with the start of the new solar cycle, and with a corresponding contraction of the polar coronal holes. This result supports the idea that the solar magnetic field controls the large scale structure of the solar wind.

It has long been known that the solar wind cannot be spherically symmetric although, perforce, this simple model has often been used. The most obvious structures are the fast streams which are now known to have steep spatial gradients both in longitude and latitude (e.g. Hundhausen 1977). We present here measurements of the latitude structure of the solar wind speed from 1971 to 1979, made using interplanetary scintillations (IPS). The results show that persistent high speed streams emanate from the poles of the sun; and that these streams are modulated by the solar cycle exactly as are the polar coronal holes.

The IPS technique has been discussed by many authors (Dennison and Hewish 1967, Armstrong and Coles 1972, Watanabe, Kakinuma, Kojima, and Shibasaki 1973). Our 74 MHz observatory at San Diego and its data analysis are described by Coles and Kaufman (1968). IPS observations in the ecliptic have been compared with direct spacecraft measurements (Coles, Harmon, Sullivan, and Lazarus 1978). That work gave a 'calibration' of the simple interpretation, which we adopt here, that the IPS method estimates the solar wind speed at the point where the maximum scattering occurs. We make IPS observations of eight radio sources daily, from which we typically obtain useful solar wind speed estimates at three to five such effective locations. The heliographic latitude of these locations spans 60°S to 70°N . However, the coverage is not continuous; northern latitudes ($> 20^{\circ}$) are observed from March-July and October-November, while southern latitudes ($> 20^{\circ}$) are observed June-July, each year (see Fig. 1 of Coles and Rickett 1979).

The solar wind speed can be averaged over longitude to provide the speed versus latitude plots of Figure 1. The characteristic U-shape has been described by Coles and Rickett (1976). This phenomenon is best

described as evidence for persistent fast streams from the north and south poles of the sun. These polar streams are the solar wind response to the polar coronal holes, in just the same way that ecliptic streams originate from low latitude coronal holes.

Long-term changes in the polar streams can be seen in Figure 1. We identify three phases.

First, 1973-75 shows stable co-rotating structures with two "polar" streams tilted about 30° from the rotation axis, as revealed in Figure 2 (Sime and Rickett 1976). The major coronal holes at this time can similarly be described as tilted polar holes; Figure 3 shows one estimate of the large coronal hole boundaries, revealing holes well aligned with the streams shown in Figure 2. Indeed the increased average speed at the equator in 1974 (Figure 1) is due to these streams, as discussed in the paper by Hundhausen (see this volume).

The second phase, 1976-77, during which solar activity is near minimum, shows polar streams that have widened and are better aligned with the rotation axis. This gives a steep average latitude gradient between 15° and 30° (over 10 km/s per degree) comparable with instantaneous measurements of the latitude gradient made by spacecraft (Smith and Rhodes 1974).

The third phase, 1978-79, occurs at the start of the new cycle of solar activity and shows a dramatic decrease in the speed at 30 - 60° N, with similar changes in the south. In other words the polar streams are narrowing at the same time that the new sunspots are emerging at mid-latitudes. This change evidently occurred at the same phase during the previous cycle. The change that we observed between 1977 and 1978 was seen by Hewish and Symonds (1969) between 1966 and 1967. However,

they observed only for two months of these two years and so were unable to draw any strong conclusions.

The presence of mid-latitude sunspots implies that bipolar magnetic regions are dominating these latitudes, restricting the area of open fields (i.e. the polar coronal holes). Evidence for the reduced area of the polar holes was given by Sheeley in the previous paper (see this volume). Figure 4 shows a comparison of average wind speed at 0, 30°, 60°N with the area of the north polar hole from 1971-79. Hole area estimates from Kitt Peak He 10830 Å data are plotted for 1974-78 together with earlier estimates from a variety of techniques. The slowing of the wind at 30° and 60°N in late 1977 to the present is closely matched by the shrinking of the north polar hole.

Figure 5 shows the comparison as a plot of latitude versus time. The continuous line in the north and horizontal bars in the south represent the boundaries between fast and slow wind from six-month averages of wind speed. They can be viewed as average boundaries of the polar streams in the north and south. The dramatic change occurs between the period 1974 to early 1977 and the period late 1977 to the present. In the earlier period the boundary is near $\pm 30^\circ$, showing that the fast polar streams filled 50% of the total 4π steradians; while in the recent period the boundary moved up to near $\pm 65^\circ$, showing that the polar stream now fills only 9% of 4π steradians. This is similar to the situation in 1971, although our data coverage for that year is poor. The various symbols identify the polar hole boundaries (on the assumption of axial symmetry). Although there are real rotation to rotation changes, the long-term behavior can be described as a 60°

boundary (13% solid angle for north plus south hole) in 1974-77, followed by a retreat to 70° (6% of solid angle) in mid-1978.

We may define a solid angle expansion ratio between the (arbitrary) 500 km/s wind speed solid angle and the solid angle defined by the He 10830 Å holes. This ratio decreased from 3.8 for the earlier period to 1.5 for 1978. Whereas the numerical value of this ratio cannot easily be related to the areal expansion factor as defined for the northern polar hole by Munro and Jackson (1977), the change in our ratio shows that the areal expansion factor of the polar holes decreased substantially as the holes shrunk.

In summary we have observed that the polar streams have narrowed substantially, at the same time that the polar holes have narrowed. This result reconfirms the importance of the solar magnetic field in controlling the corona and solar wind. It is likely that this changing three-dimensional structure determines the solar cycle modulation of cosmic rays. From the viewpoint of SCADM, it is clear that the high latitude solar wind shows a more pronounced solar cycle dependence than does the ecliptic solar wind, and should be monitored together with the sun and ecliptic solar wind. Equally important, the detailed information on the latitude structure to be obtained from the Solar Polar Mission must be viewed in the context of the long-term evolution as presented here.

We thank the Atmospheric Sciences Section of the N.S.F. for continued support under grant ATM78-06770 and previous grants; we thank AFGL for support under contract F19628-77-C-0161. We particularly thank our colleagues at UCSD who have helped with the project over the years.

Figure Captions

Figure 1. Solar wind speed measured by IPS averaged into 15° intervals in heliographic latitude for the years 1972-1978 and January-June 1979. The error bars are \pm twice the standard deviation in the average.

Figure 2. The average solar wind speed in $15^\circ \times 15^\circ$ bins of heliographic latitude and longitude coded by the grey scale as indicated. The IPS data were averaged for Carrington rotations 1612-1617 (March-July 1974).

Figure 3. Coronal holes indicated by a contour of low K-coronameter brightness (1.5×10^{-8} pB); the tick marks point toward low brightness, i.e. toward the holes. Data supplied by Drs. R. and S. Hansen (H.A.O.).

Figure 4. North polar hole area as percentage of solar surface (Sheeley, 1979); curve is drawn by eye. Solar wind speed from IPS observations averaged over six months and 15° in latitude centered on the latitudes indicated.

Figure 5. Solid curve (in the north) and horizontal bars (in the south) indicate the contour of 500 km/s average solar wind speed. The latitude boundaries of the polar holes are indicated by various symbols: \oplus He 10830 Å, \times Bohlin (1977), \bullet Broussard et al. (1978), \blacktriangle Fe 5303 Å (threshold at 1.5×10^{-6} of disc center brightness, data from Sacramento Peak Observatory).

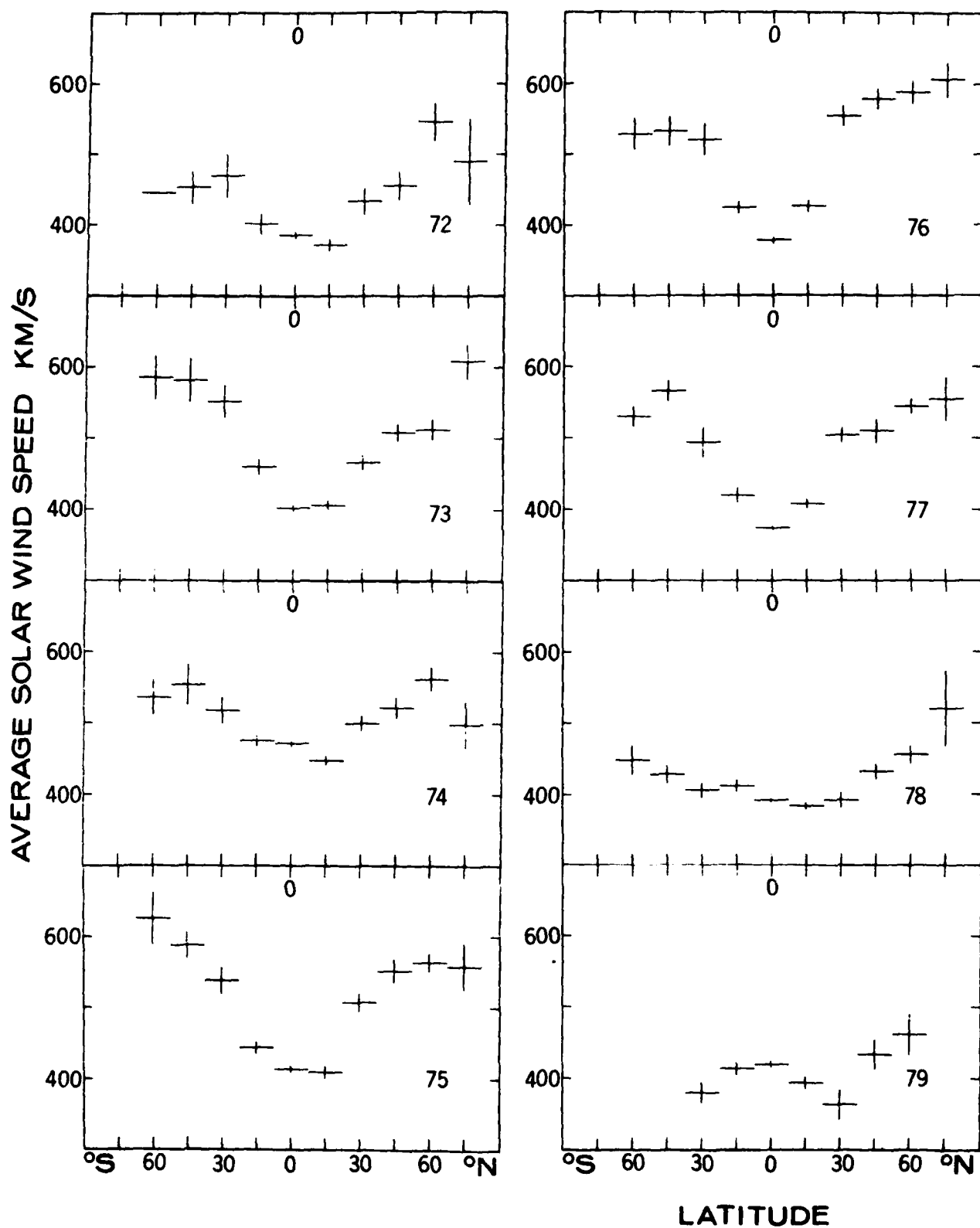


Figure 1.

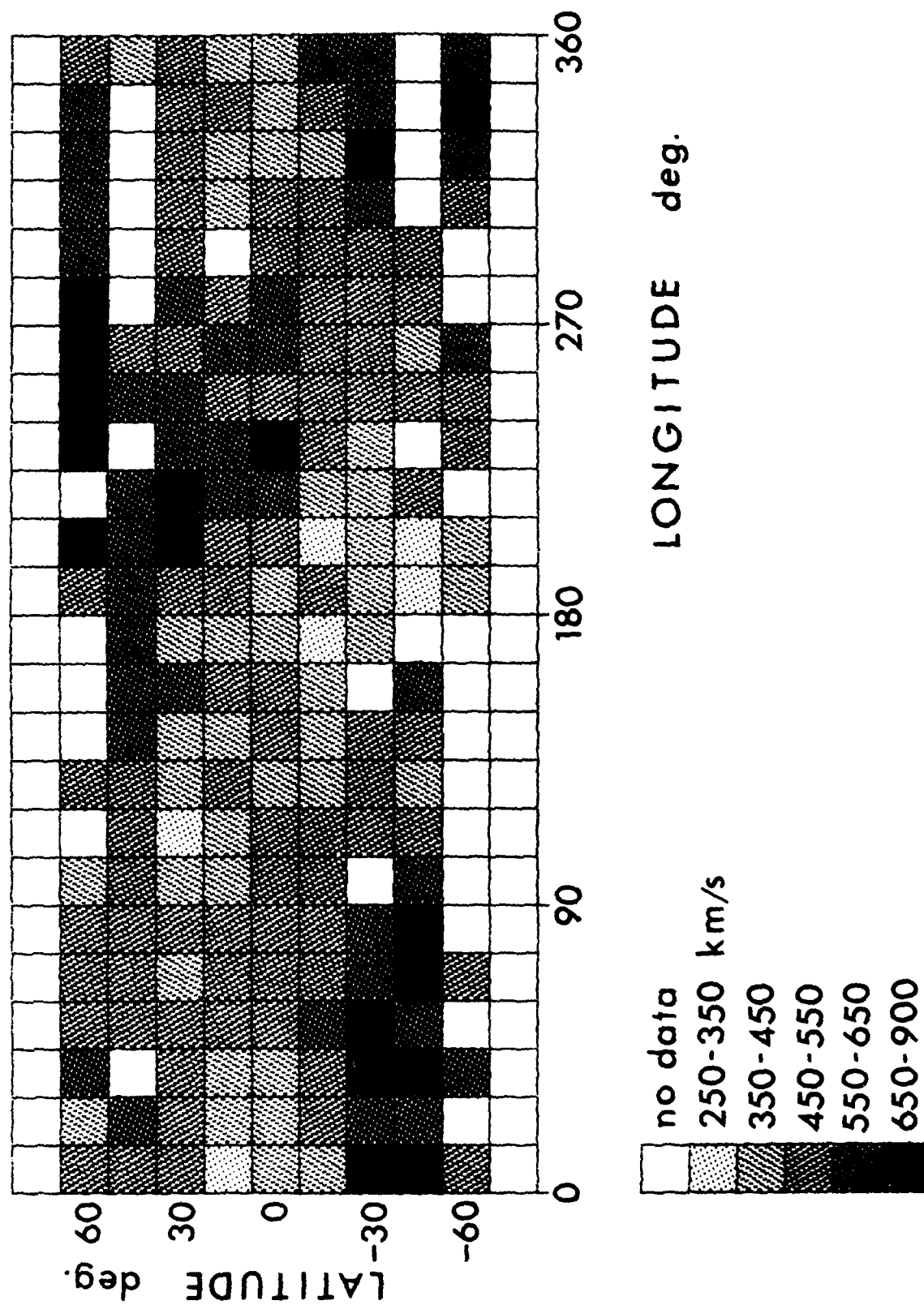


Figure 2.

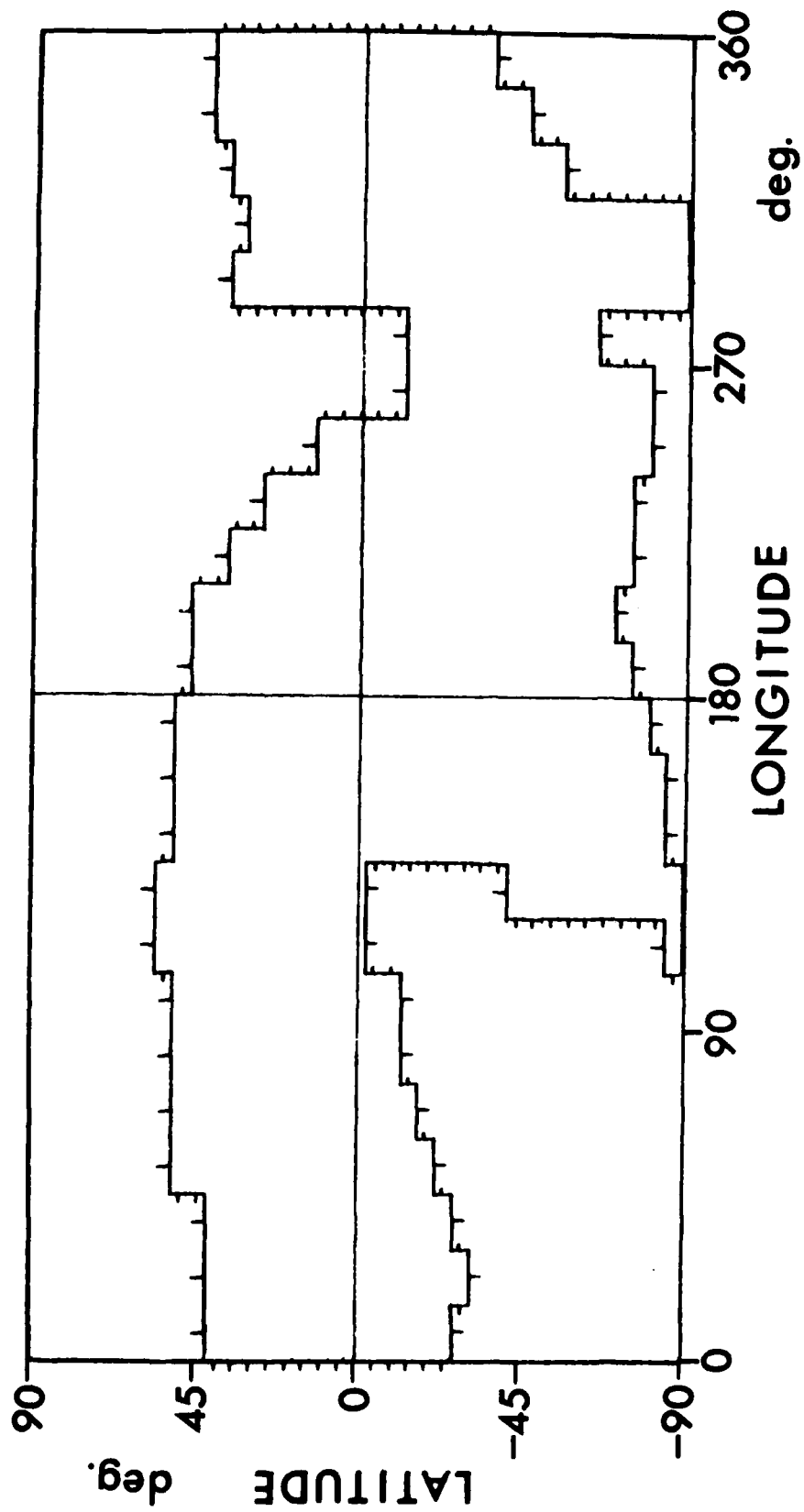


Figure 3.

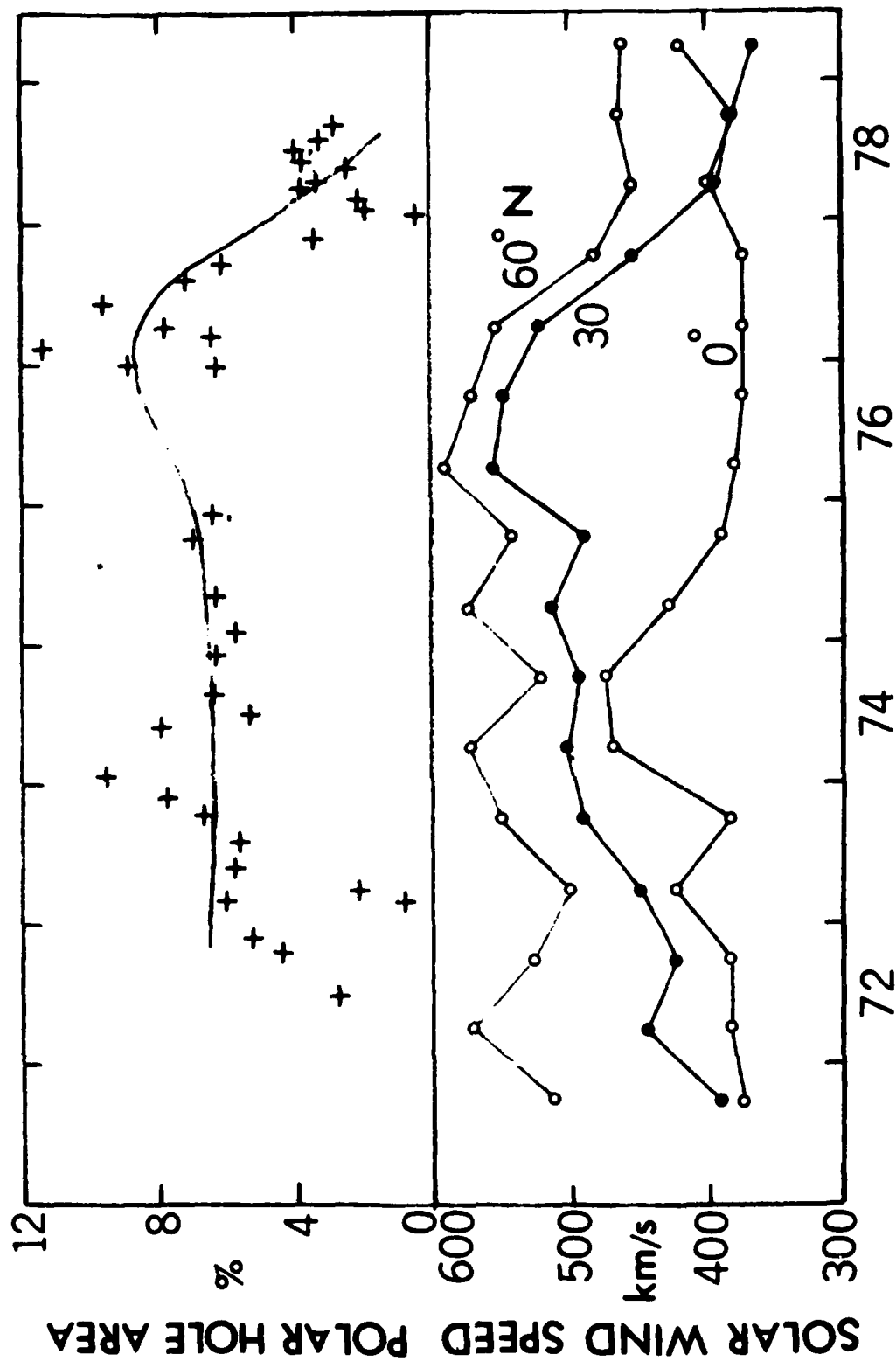


Figure 4.

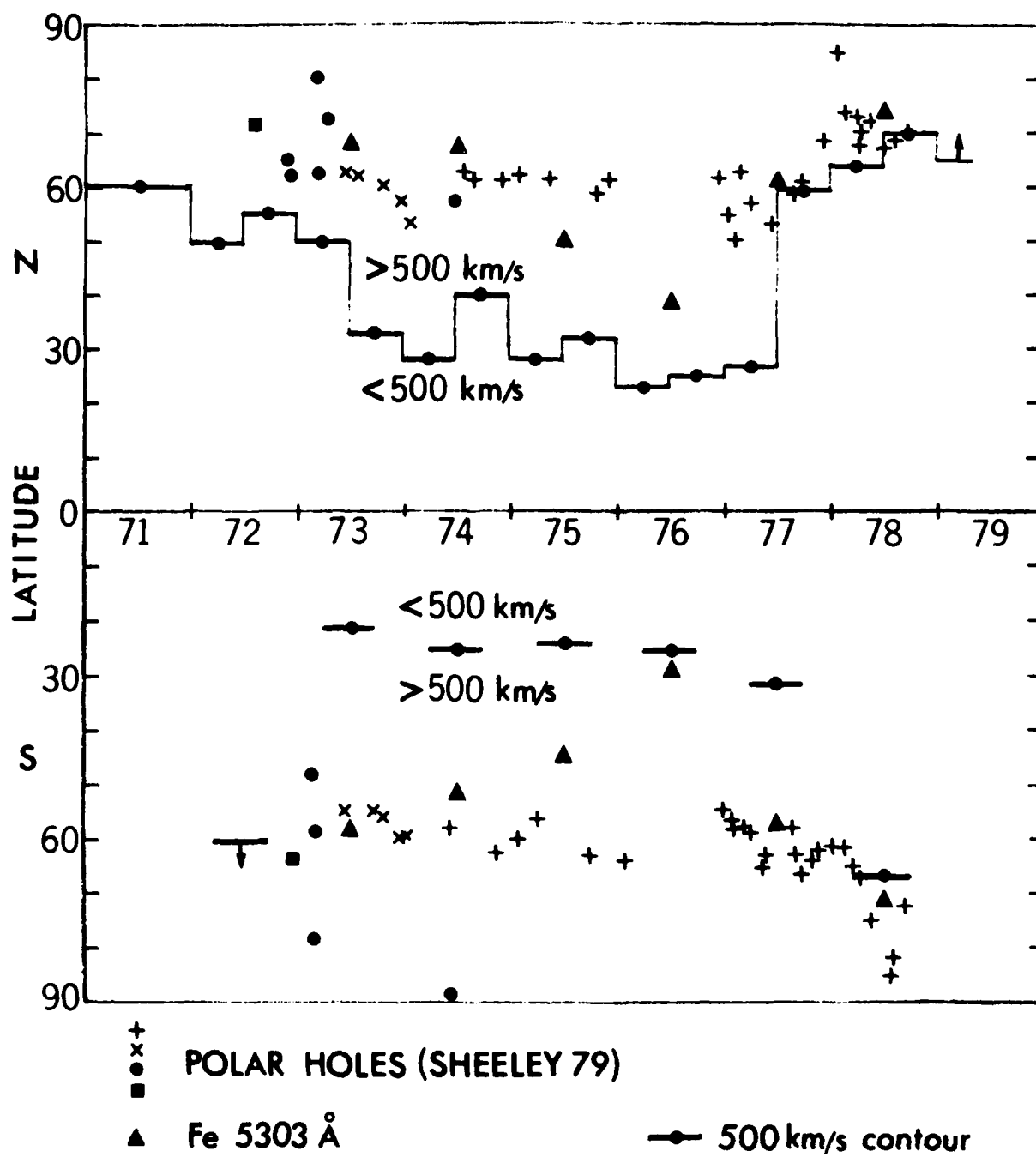


Figure 5.

References

- Armstrong, J. W., and W. A. Coles, Analysis of three-station interplanetary scintillation, J. Geophys. Res., 77, 4602, 1972.
- Coles, W. A., J. K. Harmon, A. J. Lazarus, and J. D. Sullivan, Comparison of 74-MHz interplanetary scintillation and Imp 7 observations of the solar wind during 1973, J. Geophys. Res., 83, 3337, 1978.
- Coles, W. A., and J. J. Kaufman, Solar wind velocity estimation from multi-station IPS, Radio Science, 13, 591, 1978.
- Coles, W. A., and B. J. Rickett, IPS observations of the solar wind speed out of the ecliptic, J. Geophys. Res., 81, 4797, 1976.
- Coles, W. A., and B. J. Rickett, Solar wind speed from IPS measurements at U.C. San Diego, Solar Geophysical Data, No. 402 (Supplement), 13, 1978.
- Dennison, P. A., and A. Hewish, The solar wind outside the plane of the ecliptic, Nature, 213, 343, 1967.
- Hewish, A., and M. D. Symonds, Radio investigation of the solar plasma, Planetary Space Sci., 17, 313, 1969.
- Hundhausen, A. J., An interplanetary view of coronal holes, in A Monograph on Coronal Holes, edited by J. B. Zirker, chap. 7, Colorado Associated University Press, Boulder, 1977.
- Munro, R. H., and B. V. Jackson, Physical properties of a polar coronal hole from $2 R_0$ to $5 R_0$, Ap. J., 213, 874, 1977.
- Sime, D. G., and B. J. Rickett, The latitude and longitude structure of the solar wind speed from IPS observations, J. Geophys. Res., 83, 5757, 1978.
- Watanabe, T., T. Kakinuma, M. Kojima, and K. Shibasaki, Solar wind disturbances detected by the interplanetary scintillation of radio sources in early August 1972, J. Geophys. Res., 78, 8364, 1973.

